THE JOURNAL OF BIOLOGICAL CHEMISTRY
Vol. 278, No. 52, Issue of December 26, pp. 52848–52856, 2003
Printed in U.S.A.

Characterization of the Interaction of the Stress Kinase SPAK with the Na^+-K^+-$2Cl^-$ Cotransporter in the Nervous System

EVIDENCE FOR A SCAFFOLDING ROLE OF THE KINASE*

Received for publication, August 26, 2003, and in revised form, October 13, 2003
Published, JBC Papers in Press, October 16, 2003, DOI 10.1074/jbc.M309436200

Kerstin Piechotta, Nicole Garbarini, Roger England, and Eric Delpire‡

From the Department of Anesthesiology and Center for Molecular Neuroscience, Vanderbilt University Medical Center, Nashville, Tennessee 37232

Activity of heterologously expressed NKCC1 was analyzed under basal and activated conditions in the presence and absence of binding of Ste20-related proline-alanine-rich kinase (SPAK). Mutant NKCC1 that lacks the ability to bind to this kinase showed K^+ transport function identical to wild-type NKCC1. Thus, preventing the binding of the kinase to the cotransporter does not affect cotransporter function. In contrast, several experiments suggest a possible role for SPAK as a scaffolding protein. First, Western blot analysis revealed the presence, and in some tissues abundance, of truncated forms of SPAK and OSR1 in which the kinase domains are affected and thus lack kinase activity. Second, a yeast two-hybrid screen of proteins that interact with the regulatory (binding) domain of SPAK identified several proteins all involved in cellular stress pathways. Third, p38, one of the three major MAPKs, can be coimmunoprecipitated with SPAK and with NKCC1 in an activity-dependent manner. The amount of p38 coimmunoprecipitated with the kinase and the cotransporter significantly decreases upon cellular stress, whereas the interaction of the kinase with NKCC1 remains unchanged. These findings suggest that cation-chloride cotransporters might act as "sensors" for cellular stress, and SPAK, by interacting with the cotransporter, serves as an intermediate in the response to cellular stress.

Cation-chloride cotransporters, which mediate the tightly coupled, electroneutral movement of cations (Na^+ and K^+) together with Cl^-, can be divided into Na^+-dependent transporters, such as Na-K-2Cl cotransporters (NKCC1–2) and the Na-Cl cotransporter (NCC), and Na^+-independent K-Cl cotransporters (KCC1–4). All of these transporters have a well conserved topology with large intracellular amino-terminal and carboxyl-terminal tails and 12 transmembrane spanning domains. The core protein shares some homology to amino acid permeases (for reviews see Refs. 1 and 2). A variety of stimuli regulates these transporters, including hormonal (3), cytokines (4, 5), cell volume (6, 7), oxidative stress (8), etc. There is also accumulating evidence that cation-chloride cotransporters participate in pathways leading to cell differentiation, growth and proliferation (9, 10), and apoptosis (11, 12). At the molecular level, the activation-deactivation of these cotransporters mostly involves phosphorylation/dephosphorylation mechanisms, the details of which are still the subject of intense investigation.

To identify proteins that directly interact and regulate cation-chloride cotransporters, we recently performed a yeast two-hybrid screen using the cytosolic amino-terminal tail of KCC3. We identified two closely related kinases that bind to KCC3, NKCC1 and NKCC2 (13). These kinases belong to the group of Ste20 kinases that function as regulators of MAPK[1] cascades (14). The first kinase, SPAK (Ste-20 related proline-alanine-rich kinase, or PASK, as the rat homologue), is highly expressed in epithelia and neurons (15). Its gene is located on human chromosome 2q31.1. The second kinase, OSR1, which is named based on a 30% homology to an *o*xidative *s*tress *r*esponse kinase, has much higher homology to SPAK (67%). The *OSR1* gene is located on human chromosome 3p22-p21.3 (16). There are orthologues of OSR1 in *Caenorhabditis elegans* and *Drosophila*. Inactivation of the *Drosophila* ortholog, *fray*, results in a phenotype with axonal ensheathment deficits (17).

The catalytic (kinase) domains of SPAK and OSR1 are located at the amino terminus, and the regulatory domains are at the carboxyl terminus (14). We demonstrated that the binding with cation-chloride cotransporters takes place at the extreme carboxyl termini of SPAK and OSR1 (13). The two kinases bind to peptides with a minimum of 9 residues with the following initial consensus sequence: (R/K)F*X*(V/I). This motif was found twice in the amino terminus of NKCC1, and each sequence was shown to interact with the kinases. Recently, Dowd and Forbush (18) proposed a regulatory role of SPAK (PASK) on the activity of NKCC1. They showed that overexpression of a dominant negative PASK (inactive kinase) resulted in a lack of activation of NKCC1 upon lowering the intracellular Cl^-. They also demonstrated that inactive SPAK failed to phosphorylate NKCC1 upon activation. Whether or not the kinase directly phosphorylated and activated the cotransporter still remains unclear.

In the present study, we show that preventing the interaction of SPAK and OSR1 with NKCC1 fails to influence the activity of the cotransporter under basal or activated conditions. Our results therefore suggest that binding of the kinase to the two SPAK binding domain is not required for NKCC1 activation. We demonstrate that SPAK, besides colocalizing with cation-chloride cotransporters, interacts with additional proteins that are involved in the response of the cell to stress.

* This work was supported by a grant-in-aid from the National American Heart Association and by National Institutes of Health Grant NS36758. The costs of publication of this article were defrayed in part by the payment of page charges. This article must therefore be hereby marked "*advertisement*" in accordance with 18 U.S.C. Section 1734 solely to indicate this fact.

‡ To whom correspondence should be addressed: T-4202 Medical Center North, Nashville, TN 37232-2520. Tel.: 615-343-7409; Fax: 615-343-3916; E-mail: eric.delpire@vanderbilt.edu.

[1] The abbreviations used are: MAPK, mitogen-activated protein kinase; MAP2, microtubule-associated protein 2; PVDF, polyvinylidene difluoride; PBS, phosphate-buffered saline; GFAP, glial fibrillary acidic protein; AATYK, apoptosis-associated tyrosine kinase.

Furthermore, we show that the ability of SPAK to coimmunoprecipitate p38 changes upon extracellular stress. Thus, we propose that the kinase serves as a scaffolding protein, gathering stress-response proteins in the vicinity of the cotransporters.

EXPERIMENTAL PROCEDURES

NKCC1 Function in Xenopus laevis Oocytes—The open reading frame of the mouse NKCC1 (3.7 kb) was ligated into pBF, a vector suitable for expression in amphibian oocytes. The cDNA was linearized with MluI and transcribed into cRNA using the mMESSAGE mMACHINE SP6 transcription system from Ambion. cRNA was quantitated by measurement of its absorbance at 260 nm, and its quality was verified by agarose gel electrophoresis (1% agarose, 0.693% formaldehyde). A small NarI-NcoI fragment was subcloned into the vector pBluescript (pBSK+) for site-directed mutagenesis. Complementary sense and antisense oligonucleotides containing specific mutations were synthesized and used to amplify the subclone inserted in pBSK+ (QuikChange, Stratagene). The parental DNA was digested with DpnI, a restriction enzyme that recognizes and cleaves methylated GATC sequence. After DpnI treatment, a 1-μl aliquot of the PCR was transformed into *Escherichia coli*. Several clones were isolated and sequenced between NarI and NcoI to verify proper sequence and mutation. The fragment was then re-inserted into the original NKCC1 clone in pBF and transcribed.

Stages V–VI *X. laevis* oocytes were isolated as described previously (19) and maintained at 16 °C in modified L15 medium (Leibovitz's L15 solution diluted with water to a final osmolarity of 195–200 mosM and supplemented with 10 mM HEPES and 44 μg of gentamicin). Oocytes were injected the following day with 27.5 ng of cRNA. ^{86}Rb uptakes were performed 3 days post-injection. Groups of 20 oocytes were washed once with 3 ml of isosmotic saline (96 mM NaCl, 4 mM KCl, 2 mM $CaCl_2$, 1 mM $MgCl_2$, 5 mM HEPES (pH 7.4)) and preincubated for 20 min in 1 ml of isosmotic saline containing 1 mM ouabain. The solution was then aspirated and replaced with isosmotic or hyperosmotic solutions complemented with 2–5 μCi of ^{86}Rb. The composition of the hyperosmotic solution was identical to the isosmotic solution but with an additional 50 mM sucrose. Two aliquots of 5 μl of flux solution were sampled at the beginning of the uptake and used as standards. After 1 h of uptake, the radioactive solution was aspirated, and the oocytes were washed 4 times with 3 ml of ice-cold isosmotic or hypertonic solution. Preliminary experiments have shown that the flux is linear over a 3-h period. NKCC1 flux is expressed in picomoles of K^+/oocyte/h. Statistical analysis was performed using Student's *t* test and analysis of variance.

Surface Expression of NKCC1 in X. laevis Oocytes—Groups of 20 oocytes were injected with 27.5 ng of wild-type NKCC1 or deletion mutant NKCC1 cRNA and kept at 16 °C for 3–4 days in modified L15 medium. Then, oocytes were washed with isosmotic saline (see above) and incubated for 1 h in 1 ml of isosmotic saline containing 1 mM EZ-link sulfo-NHS biotin (Pierce). After the incubation period, oocytes were washed three times with 3 ml of isosmotic saline and lysed (20 μl/oocyte) in a buffer containing 150 mM NaCl, 10 mM Tris-Cl (pH 7.4), 1 mM EDTA, 1% Triton X-100, and protease inhibitors. Lysis was achieved by incubating the oocytes for 10 min on ice in the lysis buffer, followed by trituration with a pipette, an additional 15 min of incubation on ice, and a final centrifugation step of 15,000 $\times$ *g* for 15 min. An aliquot of the supernatant was saved for protein assay (Bradford, Bio-Rad), and an equal amount of protein sample was diluted with lysis buffer to a final volume of 1 ml. Streptavidin (50 μl) was added and incubated for 2 h at 4 °C under gentle rotation. The samples were then spun and washed three times. After the final wash, streptavidin beads were resuspended into 65 μl of sample buffer containing 4% β-mercaptoethanol, heated at 50 °C for 20 min, and subjected to 7.5% SDS-PAGE and Western blot analysis.

Preparation of an OSR1-specific Antibody—Alignment of SPAK and OSR1 proteins reveals a small region within the carboxyl terminus with very low amino acid conservation (9% identity, see Fig. 1*A* of our previous publication (13)). Thus, we selected a small fragment within that particular region to create an OSR1-specific rabbit polyclonal antibody. A 74-amino acid peptide (residues 363–436) of the mouse OSR1 was PCR-amplified from IMAGE clone 5341146 and fused to glutathione *S*-transferase. The fusion protein was grown in *E. coli* and purified with glutathione-coupled Sepharose beads. Polyclonal antibodies were produced by subcutaneous injections of the entire fusion protein into two New Zealand White rabbits (Covance, Denver, PA). The antiserum from the last production bleed was affinity-purified as described previously (20).

Yeast Two-hybrid Screen—The binding domain of SPAK to cation-chloride cotransporters (amino acids 461–556) was amplified by PCR from mouse IMAGE clone 2135848 using a sense primer containing an EcoRI site and an antisense primer containing a stop codon, followed by a BamHI site. The fragment was then ligated downstream of the Gal4 binding domain in pGBDUc2 (yeast two-hybrid vector) and transformed into PJ69-4A cells (21). SPAK-containing yeast cells were subsequently transformed with a mouse brain library in pACTII (Clontech), and a total number of 18.9×10^6 clones were screened as described previously (13).

To test for interaction between SPAK and the amino terminus of NKCC1, the entire amino terminus of the cotransporter was PCR-amplified and ligated into pGBDUc2. For the mutants, NarI-SacI fragments were isolated from full-length NKCC1 mutants in pBF and exchanged with the wild-type NarI-SacI fragment in pGBDUc2.

Immunofluorescence—Two adult C57BL6 mice were deeply anesthetized with isoflurane and perfused with ice-cold PBS for 5 min and with 4% paraformaldehyde/PBS for 10 min. Brains were removed and post-fixed in 4% paraformaldehyde for 2–4 h at 4 °C. Brains were then incubated in 30% sucrose for 24–48 h at 4 °C. After cutting 10-μm sections and thaw-mounting them on Superfrost Plus slides, sections were air-dried for 1 h and stored at −80 °C. For immunolabeling, slides were warmed up on a 37 °C heating plate and further processed as described previously (22). Briefly, sections were permeabilized in 1% SDS in PBS containing 8% β-mercaptoethanol, blocked with PBS, 1% bovine serum, 4% goat serum (blocking solution), and incubated overnight at 4 °C in blocking solution containing SPAK-purified polyclonal antibody (1:200; for preparation of SPAK-specific antibody see Ref. 13). After washing in high salt PBS and PBS and blocking in blocking solution, sections were exposed to the secondary antibody (Cy3-conjugated goat anti-rabbit immunoglobulin G (IgG); Jackson ImmunoResearch, West Grove, PA) at a dilution of 1:1600 for 1 h. After washing in high salt PBS and PBS, sections were mounted with Vectashield (Vector Laboratories, Burlingame, CA). For double labeling experiments, sections coming out of the washing steps were blocked in blocking solution and then incubated at 4 °C overnight at a concentration of 1:200 with either anti-glial fibrillary acidic protein (GFAP; ICN clone GA-5) to identify astrocytes or anti-microtubule-associated protein 2 (MAP2; clone A20, Roche Applied Science) to identify neurons. These antibodies were visualized with fluorescein isothiocyanate-conjugated anti-mouse IgG (1:1600; Jackson ImmunoResearch). The same protocol as for single labeling was used. We have demonstrated recently (13) the specificity of the SPAK antibody by Western blot analysis. As negative controls, immunolabeling of adjacent sections was performed omitting the first antibody, or both antibodies. The latter revealed a punctate staining in the cytosol of some cells, which we just excluded as a sign for a SPAK-positive structure. Sections were analyzed on a Zeiss Axiovert S100 microscope equipped with a Photometrics Coolsnap^{Cf} CCD camera (Roper Scientific, Tucson, AZ) connected to a G4 Apple computer.

Tissue Distribution Analysis—Tissues from two adult C57BL6 mice were promptly isolated and frozen in liquid nitrogen. One gram of tissue was homogenized in 10 ml of solution sucrose buffer (0.32 M sucrose, 5 mM Tris-HCl (pH 7.5), 2 mM EDTA) with a Teflon pestle. The homogenates were spun at 3000 rpm for 20 min, 9000 rpm for 20 min, and 32,000 rpm for 45 min. The high speed pellet consisting of microsomal protein was resuspended in a buffer containing 5 mM Tris-HCl (pH 7.5) and 2 mM EDTA. After protein quantitation using a Bio-Rad Bradford assay, equal amounts of protein were denatured, resolved on 7.5% SDS-polyacrylamide gel, and subjected to Western blot analysis.

Coimmunoprecipitation and Western Blot Analyses—Mouse brains (~400–500 mg) were dissected on ice and cut sagitally into two halves. The first half was homogenized promptly in 5 ml of lysis buffer (100 mM NaCl, 50 mM NaF, 2 mM EDTA, 150 mM Na_3VO_4, 0.5% Triton X-100, 10 mM Na_2HPO_4/NaH_2PO_4 (pH 7.2), and protease inhibitors) with a Teflon pestle and kept on ice, and the second half was cut into small chunks and incubated in oxygenated aCSF for 30 min. The composition of aCSF was as follows (in mM): 150 NaCl, 5 KCl, 0.5 $CaCl_2$, 1 $MgCl_2$, 10 glucose, 17 sucrose, 10 HEPES (pH 7.4). Because the thickness of the chunks prevents oxygen diffusion, the brain tissue becomes ischemic as demonstrated by the 10–20-fold activation of phospho-p38. After incubation, the chunks were homogenized in lysis buffer and incubated on ice for 30 min. Brain homogenates were then centrifuged at 9000 rpm for 10 min, and the supernatant was recovered. Coimmunoprecipitations were performed by incubating 1 ml of brain lysate aliquots with 10–20 μl of immunopurified antibodies (rabbit polyclonal NKCC1 (23), SPAK (13), p38 against residues 341–360 of human p38 MAPK (from Calbiochem), and mouse monoclonal anti-phospho-p38 MAPK Thr-180/Tyr-182 (Cell Signaling), under gentle rotation, overnight at 4 °C, followed by the addition of 30 μl of protein A-agarose for 2 h at 4 °C. After three washes in lysis buffer, the immunoprecipitate-agarose beads complexes

FIG. 1. **Amino acid sequence of the amino-terminal tail of the mouse NKCC1.** The sequence shows the two SPAK binding domains (9 residues each), the PP1-binding motif (4 residues), and the large peptide fragment (starting and ending with GP residues, encoded by two codons forming ApaI sites) that is deleted in our deletion mutant, and three threonine residues involved in phosphorylated regulation of NKCC1 (25).

were resuspended in loading buffer and denatured at 50 °C for 20 min. After brief centrifugation, the immunoprecipitates were resolved by 7.5% SDS-PAGE and electroblotted onto polyvinylidene difluoride (PVDF) membranes. Membranes were blocked for 2 h at room temperature with 5% non-fat dry milk in TBST (TBST, 150 mM NaCl, 10 mM Tris-HCl, 0.5% Tween 20 [polyoxyethylene-sorbitan monolaurate]). Membranes were then subjected to affinity-purified NKCC1, SPAK antibodies (1:1000) in TBST, 5% non-fat dry milk overnight at 4 °C, washed extensively in TBST, and incubated for 1 h with horseradish peroxidase-conjugated secondary antibody in blocking solution (1:4000). After extensive washing, protein bands were visualized by chemiluminescence (ECL Plus, Amersham Biosciences).

RESULTS

NKCC1 Mutants—As indicated in Fig. 1, two SPAK binding domains can be found in the amino terminus of NKCC1. The first domain, RFQVDPESV, is located 76 residues downstream of the start methionine. The second motif, RFRVNFDPA, is located 48 residues downstream of the first motif and overlaps with a putative PP1-binding motif (24). By using the yeast two-hybrid method, we demonstrated that these two minimal motifs constitute sites of interaction with the kinases SPAK and OSR1 (13). We also demonstrated previously that mutations of the phenylalanine residue at position 2 or the valine residue at position 4 to alanine completely abolished the interaction. Note that the SPAK/OSR1-binding sites are located far upstream of the threonine residue (Thr-211 for mouse NKCC1) essential for transport (25). By using site-directed mutagenesis, we produced several NKCC1 mutants and tested their function in *X. laevis* oocytes. The first mutant inactivates the first SPAK binding domain by replacing the Phe residue with Ala. Fig. 2*A* shows that this manipulation did not affect NKCC1 function, as measured as $^{86}Rb^+$ fluxes in isotonic (195 mosM) or hypertonic (265 mosM) solutions. For the second mutant, we mutated RV into AA, a mutation that prevents SPAK interaction and also affects PP1 binding (24). This second manipulation also failed to affect NKCC1 transport activity, which was in this case assessed in isotonic, hypertonic, and low Cl^- conditions (Fig. 2*B*). Because the binding of SPAK to a single motif might be sufficient to regulate NKCC1, we created a double mutant (Phe → Ala and RV → AA mutations in the first and second motif, respectively). When SPAK interaction with NKCC1 is prevented, the fluxes in isotonic, hypertonic, and low Cl^- are still identical to the ones obtained with wild-type NKCC1 (Fig. 2*C*). To confirm that the double mutant results in a loss of SPAK-cotransporter interaction, we performed separate yeast two-hybrid tests with SPAK and the wild-type NKCC1-NT, the two single mutants, and the double mutant. As shown in Fig. 3, all clones but the double mutant showed interaction with the stress kinase. In contrast to the double

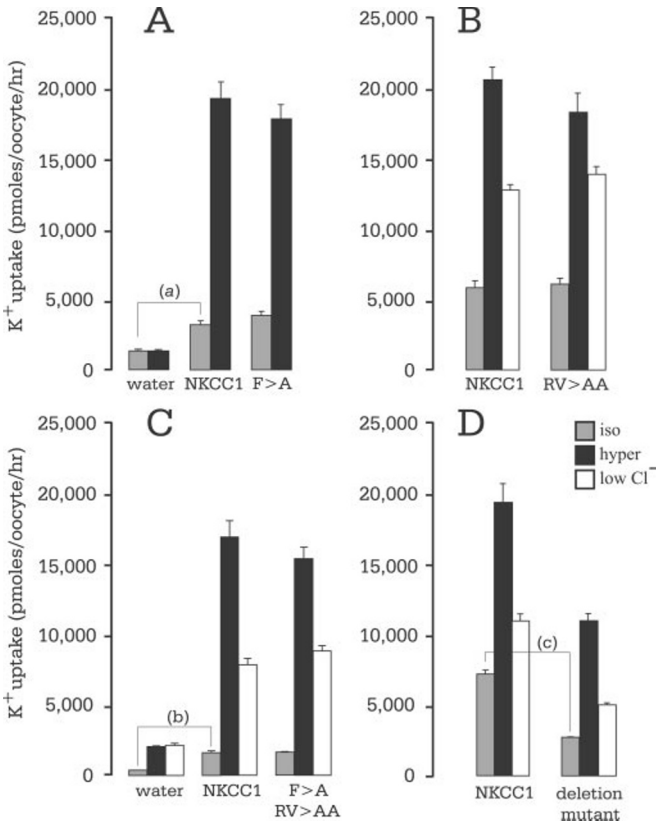

FIG. 2. **Activity of NKCC1 and NKCC1 mutants in *X. laevis* oocytes.** *A*, comparison between water-, NKCC1-, and NKCC1[F>A]-injected oocytes incubated in isotonic (*gray bars*) or hypertonic (*black bars*) solutions. *B*, comparison between NKCC1- and NKCC1[RV>AA]-injected oocytes incubated in isotonic, hypertonic, or low internal Cl^- (*white bars*) conditions. *C*, comparison between water-, NKCC1-, and NKCC1 double mutant-injected oocytes incubated in isotonic, hypertonic, or low internal Cl^- conditions. *D*, K^+ uptakes in wild-type and deletion mutant NKCC1 measured in isotonic, hypertonic, or low internal Cl^- conditions. *a* and *b*, K^+ uptake in NKCC1-injected oocytes is significantly different from the one measured in water-injected oocytes (analysis of variance between isosmotic conditions: $p < 0.001$); *c*, K^+ flux in deletion mutant is significantly smaller than in wild type (*t* test, $p < 0.0001$). Fluxes are expressed in pmol of K^+ per oocyte per h. Each *bar* represents the mean ± S.E. ($n = 20$ oocytes). Each *panel* represents a typical experiment, and each experiment was repeated at least once. Absolute K^+ uptake values vary from experiment to experiment.

mutant, a deletion of a large fragment containing both SPAK/OSR1 binding domains as well as a long polyalanine stretch inbetween significantly reduced NKCC1 activity (60% decrease) under isotonic, hypertonic, and low Cl^- conditions. However, the percent activation by hypertonicity and low Cl^- compared with wild type was unchanged (Fig. 2*D*). To assess whether the observed overall decrease in NKCC1 activity results from a decrease in NKCC1 trafficking, we injected groups of 20 oocytes with wild-type NKCC1 and deletion mutant NKCC1. Three days post-transfection, the oocytes were biotinylated, washed, and lysed. Western blot analysis of biotinylated protein (surface protein) with NKCC1 antibody revealed a higher number of cotransporter in the membrane for the mutant cotransporter, compared with wild-type NKCC1 (see Fig. 4). Effects of the single and double mutations were also tested while coexpressing mouse SPAK cDNA in *X. laevis* oocytes to ensure that the level of endogenous OSR1 is not a limiting factor. As with the uptakes shown in Fig. 2, there were no significant differences between the activity of mutants and wild-type NKCC1 proteins in SPAK coexpressing oocytes (data not shown). These data indicate that preventing SPAK/OSR1 interaction with NKCC1 by preventing the binding has no

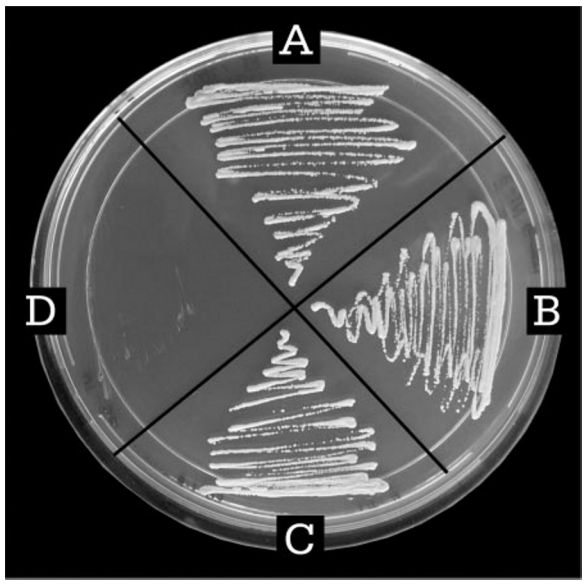

FIG. 3. **Effect of NKCC1 mutations on SPAK binding, as revealed by yeast two-hybrid analysis.** *A*, the positive interaction between SPAK and the amino terminus of NKCC1 promotes growth of the yeast in plates lacking histidine, leucine, and uracil and containing 3-amino-1,2,4-triazole. *B* and *C*, similar interaction between SPAK and each single NKCC1 mutant. *D*, absence of growth (interaction) in yeast transfected with SPAK and double NKCC1 mutant.

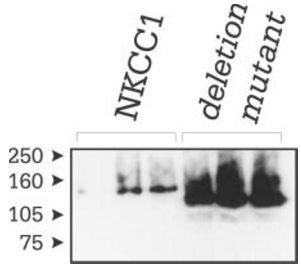

FIG. 4. **Western blot analysis of biotinylated (streptavidin bead-bound) NKCC1 protein isolated from *X. laevis* oocytes.** Three groups of 20 oocytes expressing wild-type and deletion mutant NKCC1 were treated with EZ-Link sulfo-NHS biotin, washed, and lysed. Biotinylated (surface) proteins were isolated using streptavidin beads and separated on a 7.5% SDS-polyacrylamide gel. Experiment was repeated once with identical results.

effect on NKCC1 transport activity. Therefore, our data point to a function for SPAK/OSR1 interaction with NKCC1, other than modulation of cotransporter activity.

Tissue Distribution of SPAK and OSR1—The tissue distribution of OSR1 and SPAK was examined by Western blot analysis using an OSR1-specific polyclonal antibody and a SPAK polyclonal antibody (13). As shown in Fig. 5, SPAK and OSR1 are expressed in all tissues examined, with the exception of the salivary gland that failed to show OSR1 immunoreactivity. Several observations can be made from this tissue distribution. 1) both SPAK- and OSR1-specific antibodies react with two major bands: a band of ~50 kDa molecular size and a larger band of ~60 kDa. 2) The high SPAK band is generally more abundant than the lower SPAK band, and the reverse is observed for OSR1 with the lower molecular weight band frequently being more abundant than the higher one. 3) Tissues such as brain, testis, stomach, and salivary gland express SPAK in higher abundance than lung, kidney, liver, muscle, and heart. In contrast, the tissues with highest OSR1 protein were lung, muscle, and testis when compared with brain, kidney, stomach, heart, and salivary gland.

The predicted molecular size of OSR1 (58.3 kDa, 527 residues) is smaller than the calculated molecular size of SPAK

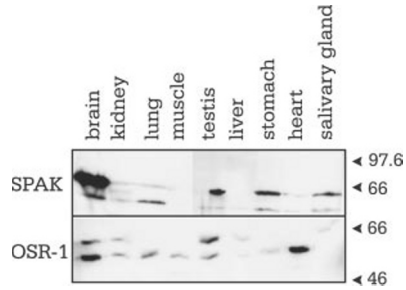

FIG. 5. **Distribution of SPAK and OSR1 in mouse tissues.** Microsomal proteins (60 μg) were separated on 7.5% SDS-PAGE, transferred to PVDF membranes, and subjected to Western blot analysis using anti-SPAK and anti-OSR1 antibodies. Each antibody recognizes two major bands in the range of 45–60 kDa. Note the abundance of SPAK expression in the brain compared with other tissues. Tissue distribution of SPAK and OSR1 was repeated once with identical results.

(60.3 kDa, 556 residues). To establish that the presence of two major reactive bands observed on Western blots with the SPAK and OSR antibodies is not due to antibody cross-reactivity, we separated kidney proteins on 7.5% SDS-polyacrylamide gel, transferred onto nylon membrane, and cut the membrane right in the middle of the loaded lane. Each half-membrane was probed with one antibody. As seen in Fig. 6*A*, the sizes of the large molecular bands and low molecular bands are unambiguously different for SPAK and OSR1. This clearly suggests that there are two distinct SPAK and two distinct OSR1 proteins. Analysis of the SPAK and OSR1 sequences revealed the presence of downstream second Kozak consensus sequences in both proteins (see Fig. 6*C*). Initiations at the first methionine give full-length proteins of 60.3 and 58.3 kDa for SPAK and OSR1, respectively. In contrast, translation initiation at the second methionine results in truncated proteins of 49.2 and 52.1 kDa, respectively. Our results of Figs. 5 and 6*A* are consistent with the hypothesis of two translation initiation sites since the Western analysis clearly shows that the size difference between large and small bands is larger for SPAK than for OSR1. Furthermore, the second translation initiation site for OSR1 is a slightly better Kozak consensus than the first (Fig. 6*B*), consistent with the higher abundance of the lower protein band. These results suggest that truncated SPAK and OSR1 kinase-inactive proteins are expressed in tissues.

Expression of SPAK in the Brain, Spinal Cord, and Sciatic Nerve—SPAK was localized in brain, spinal cord, and sciatic nerve using the immunopurified anti-SPAK antibody, which we characterized previously (13). As negative controls, the primary antibody (SPAK) was omitted from the immunostaining protocol on a series of brain sections adjacent to the ones labeled with SPAK (a typical control is shown in Fig. 8*C*). The strongest SPAK immunolabeling was found on the apical membrane of epithelial choroid plexus cells (Fig. 7*A*), as described previously (13). We also found prominent staining for SPAK at the nodes of Ranvier in teased sciatic nerve (Fig. 7*B*), corresponding to the nodal expression of NKCC1 (26). In the spinal cord, cells in both the white matter and the gray matter were labeled (Fig. 7, *C–E*). Double staining of spinal cord sections with anti-SPAK and anti-MAP2 antibodies shows that neurons as well as glia cells are positive for SPAK; adjacent to motor neurons in the ventral horn in the gray matter we detected smaller cells with the solely red fluorescence caused by the anti-SPAK-Cy3 conjugate (Fig. 7*F*). We tested the entire brain for SPAK expression and found significant labeling only in the brain stem. The schematic drawing in Fig. 7*G* indicates the location of nuclei shown in Fig. 7, *H* and *I,* and the position of the section on a rostro-caudal axis (Fig. 7*G*, *inset*). A moderate signal was observed in the nucleus of the hypoglossus (Fig. 7*H*)

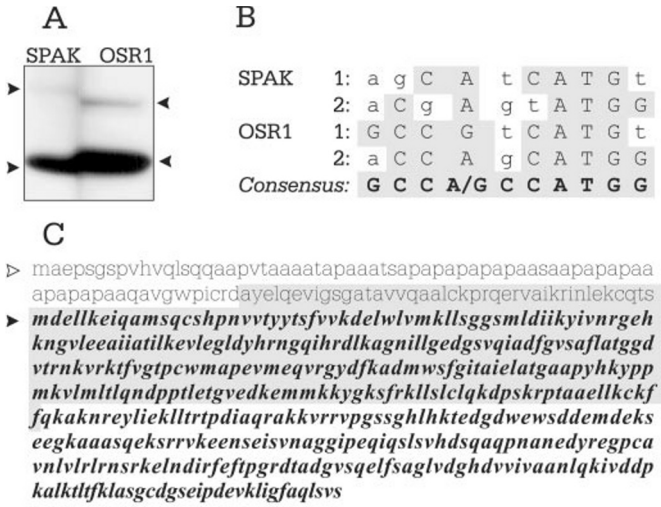

FIG. 6. **Evidence for two translational start sites in mouse SPAK and OSR1.** *A*, Western blot analysis of 60 μg of kidney protein with SPAK and OSR1 antibody. After transfer to PVDF membranes, the lane was cut in the middle to precisely size the SPAK and OSR1 bands. Note that the SPAK and OSR1 bands do not correspond and that the distance between the larger and lower molecular size bands for SPAK is larger than for OSR1. *B*, consensus sequences for both initiation-of-translation sites for SPAK and OSR1. *C*, amino acid sequence of SPAK showing the two putative start sites. The *shaded box* represents the kinase domain. Note that the second methionine truncates the kinase domain.

and in the inferior cerebellar peduncle (Fig. 7*I*, *icp*). The strongest labeling in the brain stem was found in the spinal tract of the trigeminal nerve (Fig. 7*I*, *sp5*) along its entire extension (Fig. 7, *I* and *L*, and Fig. 8*B*). In sections further rostral (Fig. 7*J*), we found moderate immunolabeling in the motor neurons of the facial nerve (Fig. 7*K*), in cells of the dorsal (Fig. 7*M*, *DCN*) as well as ventral cochlear nuclei (Fig. 7*N*, *VCN*), and in giant reticular neurons (Fig. 7*O*). A faint signal was observed in the vestibulocochlear nerve (Fig. 7*L*). The most rostral sections containing significantly SPAK-immunolabeled structures still derived from the brain stem (Fig. 8*A*). Within this area, the strongest signal was detected in the aforementioned sp5 (Fig. 8*B*). The adjacent brain section was not exposed to the primary antibody (negative control) and was devoid of labeling (Fig. 8*C*). Cells in the medial nucleus of the trapezoid body (*MNTB*) were positive for SPAK (Fig. 8*D*) and were identified as neurons by double-labeling with MAP2 antibody (Fig. 8, *E* and *F*). Other auditory structures that were moderately labeled were the lateral nucleus of the trapezoid body (Fig. 8*G*, *LNTB*), the anterior ventral cochlear nucleus (Fig. 8*H*, *AVCN*), as well as the posterior ventral cochlear nuclei (not shown). SPAK labeling was also found in motor neurons of the trigeminal nerve (Fig. 8*I*). In contrast to the 8th cranial nerve, which was SPAK-immunolabeled (Fig. 8*J*), no staining was found in the 7th nerve as shown by the lack of staining in Fig. 8*K* and by the double labeling of the same section with SPAK and GFAP in Fig. 8*L*. These results suggest that SPAK is expressed in the gray and white matter of the spinal cord, the nodes of Ranvier in the sciatic nerve, and in several brain stem structures. More rostral areas were devoid of signal except for the choroid plexus. Furthermore, SPAK expression was shown in both neuronal and glial cells.

Yeast Two-hybrid Screen of a Mouse Brain Library with the Carboxyl-terminal Binding Domain of SPAK—To better delineate the functional pathway linking cation-chloride cotransporters to SPAK, we sought to identify additional binding partners of the kinase. We screened a yeast two-hybrid mouse brain library (cDNAs inserted in pACT2) by using the binding domain of SPAK as a bait. From 18.9×10^6 clones plated on growth restrictive substrate (−uracil, −leucine, and −histidine), we isolated 139 clones that survived several rounds of selection. From these surviving clones, we identified several SPAK-binding partners, some of which were identified multiple times through independent cDNA clones (see Table I). For instance, apoptosis-associated tyrosine kinase (AATYK) was identified 7 times through 4 distinct cDNA clones, one of which was isolated 4 times. One interactor isolated several times was identified through BLAST searches as 5E5 antigen using the NCBI data base and as a tyrosine kinase using the mouse Celera data base. This novel Celera protein contains a typical tyrosine kinase domain. Its alignment with AATYK revealed an overall 29% homology with several regions of high conservation, indicating a relationship between the two proteins. Analysis of the amino acid sequence of these clones revealed the presence of SPAK-binding motifs. Again for the apoptosis-associated tyrosine kinase, we identified three sequences within the carboxyl terminus that resemble the SPAK-binding motif. These sequences were RFEWDGDFP, RFTVSPTPA, and RFSITHISD. We tested all three sequences for interaction with SPAK by using the yeast two-hybrid assay, and only the last 2 clones, which conform to the previously described motif (R/K)FX(V/I), yielded positive interaction. Note that most of these interactors are involved in the response of cells to osmotic, oxidative, and other stresses.

Coimmunoprecipitation of SPAK, NKCC1, and p38—To examine further the relationship between NKCC1, SPAK, and cellular stress, we isolated proteins from control brain and ischemic brain tissue, which was exposed to non-carboxygenated aCSF, and performed coimmunoprecipitation experiments. Evidence for ischemic stress was verified by the marked activation of phospho-p38 (Fig. 9*A*, *pp38*). The figure panel also shows that the amount of NKCC1 and SPAK coprecipitated with pp38 decreases with cellular stress. In contrast, the amount of SPAK coprecipitated with NKCC1 does not change significantly with stress. Of interest is the observation that only the larger molecular form of NKCC1, which represents phosphorylated NKCC1, interacts with pp38. Indeed, Fig. 9*B* shows two distinct NKCC1 bands in the NKCC1 immunoprecipitate, with the lower molecular size much more abundant than the higher molecular size. Only the larger band is observed in a pp38 immunoprecipitate run in the same gel in an adjacent lane. These data suggest that NKCC1, SPAK, and p38 form a complex and that p38 or pp38 but not SPAK is released upon cellular stress.

DISCUSSION

In an effort to characterize the SPAK/OSR1-binding site, we have shown previously by alanine-scanning mutagenesis on KCC3 and NKCC2 motifs that a mutation of the phenylalanine residue at position 2 or the valine residue at position 4 into alanine completely disrupted SPAK interaction with these cotransporters (13). The absence of interaction was also verified by glutathione *S*-transferase pull-down assays. In the present study, we created several NKCC1 mutants disrupting either one or both binding motifs that we had identified previously at the amino terminus of NKCC1, and we examined their transport activity in *X. laevis* oocytes. Our rationale was as follows: if the kinase interacts and phosphorylates NKCC1, thus leading to a change in its activity, preventing the kinase from interacting with the cotransporter should prevent activation of transport. Fig. 3 demonstrates that the two SPAK-binding motifs are functional binding sites; mutation of either one alone does not preclude interaction, whereas the double mutant shows a complete absence of interaction. Our flux experiments demonstrate that a double mutant cotransporter that is unable

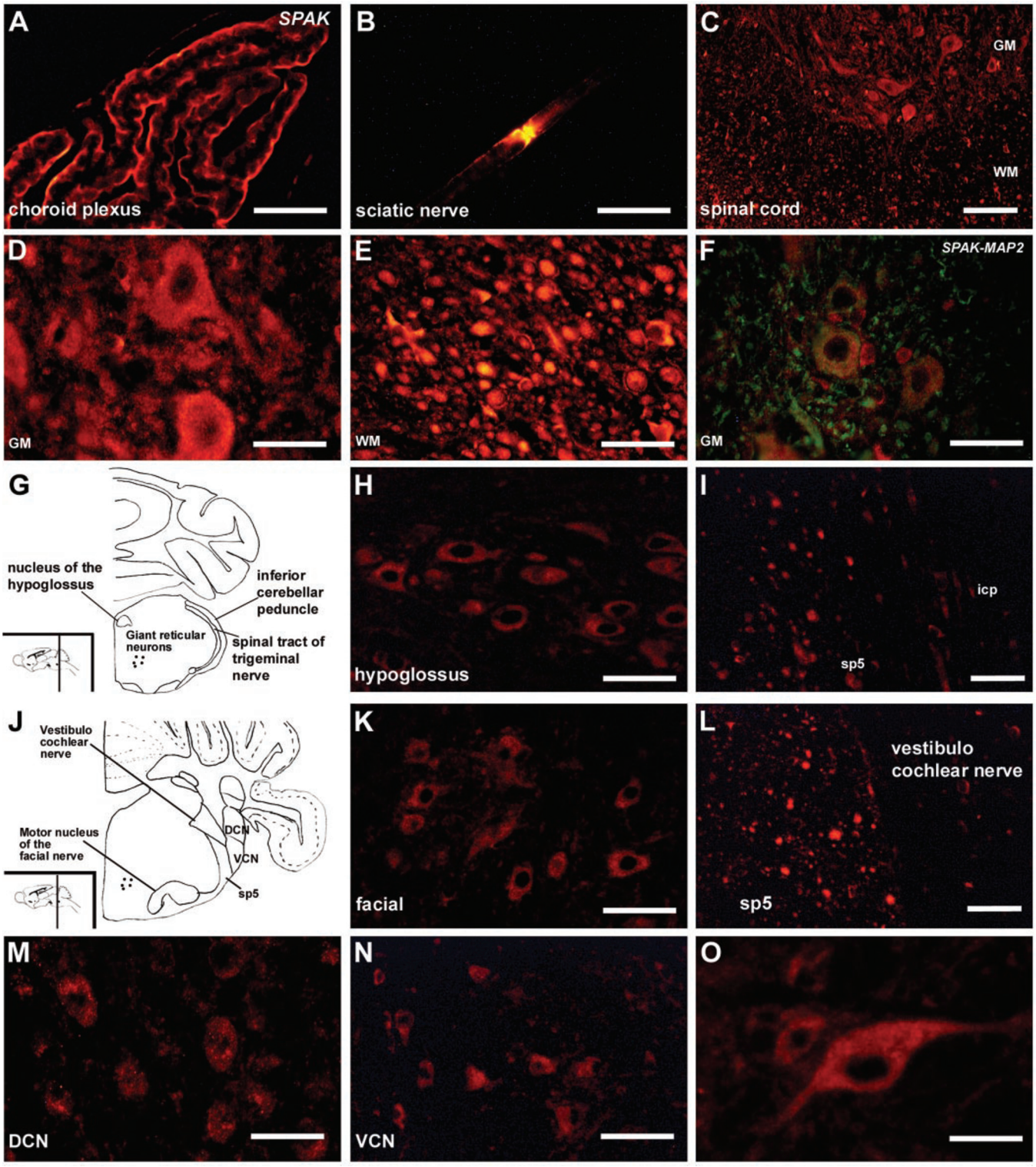

FIG. 7. *A*, immunohistochemical labeling of brain slices with anti-SPAK antibody was strongest on the apical membrane of epithelial choroid plexus cells. *B*, SPAK immunolabeling at the node of Ranvier of teased sciatic nerve. *C–E*, in the spinal cord, cells in both the white matter (*WM*) and gray matter (*GM*) were immunolabeled. *F*, double staining of motor neurons in the ventral horn of the spinal cord with anti-SPAK and anti-MAP2. Note the exclusively SPAK-stained glial cells adjacent to the motor neurons. *G* and *J*, schematic drawing of brainstem slices indicating the positions of SPAK-positive nuclei shown in the following pictures. *Insets* in *G* and *J*, the *vertical line* indicates the plane of the slice on a rostro-caudal axis. *H–O*, SPAK immunolabeling was detected as follows: *H*, motor neurons of the hypoglossus; *I*, the spinal tract of the trigeminal nerve (sp5); *K*, motor neurons of the facial nerve; *L*, the vestibulocochlear nerve; *M*, the dorsal cochlear nucleus (*DCN*); *N*, the ventral cochlear nucleus (*VCN*); *O*, giant reticular neurons. *Scale bars*: 30 μm in *A* and *B*, *D–F*, *H*, *K*, and *M–O*; and 100 μm in *C*, *I*, and *L*.

to interact with the kinase is fully functional and activable to the same degree by hyperosmotic and low internal Cl^- stimuli as wild-type NKCC1. Our approach is independent of a distinction between endogenously expressed SPAK in oocytes *versus* heterologously coexpressed SPAK, since the binding preventing mutation is on the cotransporter. In addition, the activity of NKCC1 and its correct expression can be directly monitored via the flux studies. In our assay system, which differs from Dowd

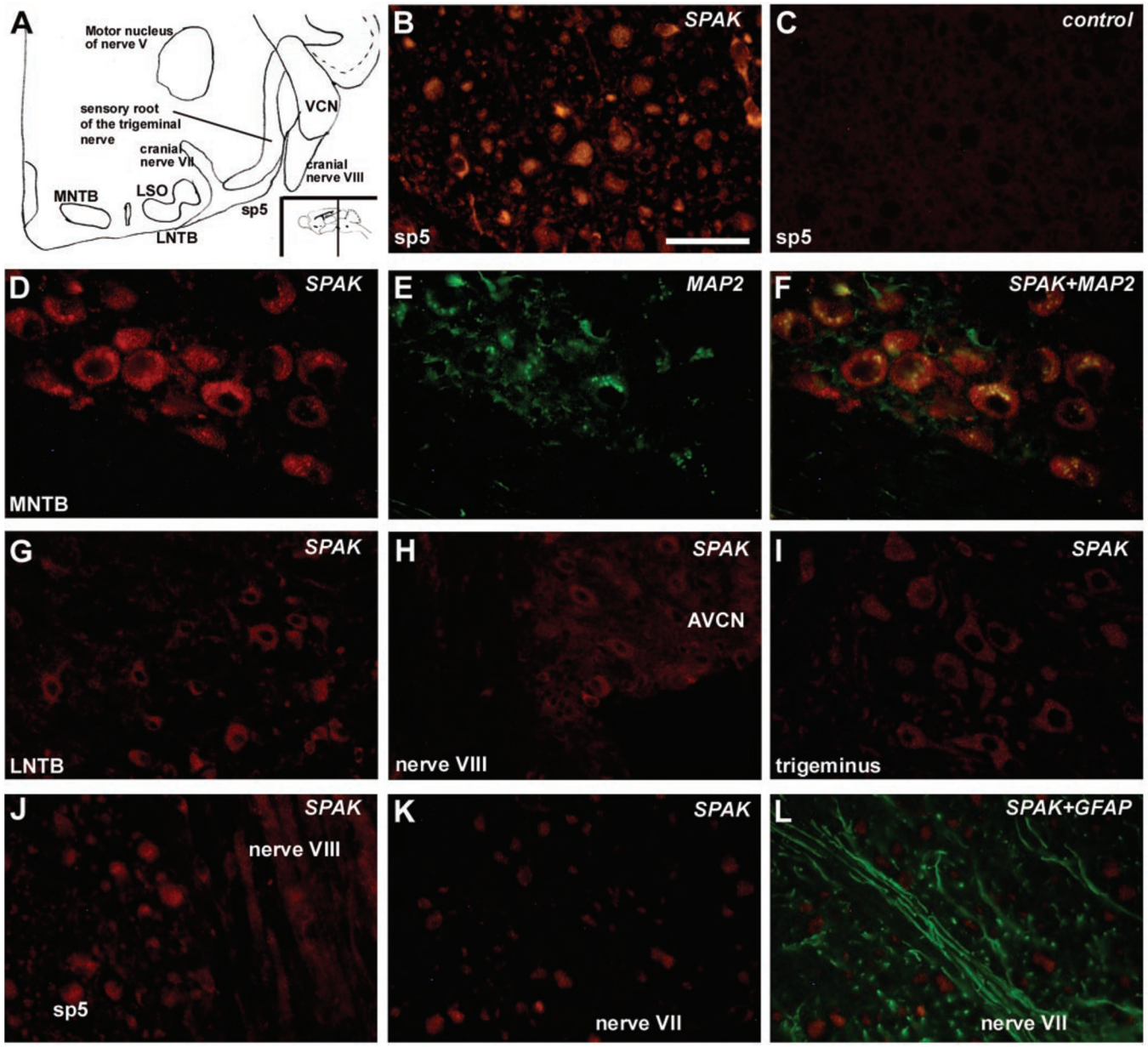

FIG. 8. *A*, schematic drawing of brainstem slice locating SPAK positive structures shown in the following pictures. The *vertical line* in the *inset* indicates the plane of the slice on a rostro-caudal axis. *B*, in the brainstem, SPAK immunolabeling was most intense in the spinal tract of the trigeminal nerve (*sp5*). *C*, the adjacent control section, shows no staining above background. *D*, moderate SPAK labeling was detected in the medial nucleus of the trapezoid body. *E*, staining for MAP2 of the same slice shown in *D*. *F*, superimposing pictures from *D* and *E*, identifies SPAK-positive cells as neurons. SPAK labeling was also found as follows: *G*, in the lateral nucleus of the trapezoid body (*LNTB*); *H*, anterior ventral cochlear nucleus (*AVCN*); *I*, motor neurons of the trigeminal nerve; and *J*, the auditory nerve (*VIII nerve*). *K*, the trigeminal nerve (*VII nerve*) is devoid of SPAK immunolabeling. *L*, same section as in *K*. Double staining of the VIIth nerve with anti-SPAK and anti-GFAP antibodies. *Scale bar*: 30 μm in *B* (for *B–I*).

and Forbush (18), we were thus unable to demonstrate functional changes. These authors had recently reported a reduction of human and shark NKCC1 activity by overexpressing the kinase negative, dominant negative PASK mutant. Differences between the two sets of data could originate from differences between HEK293 cells and *X. laevis* oocytes. However, this would suggest that different regulatory proteins (*e.g.* kinases) and separate regulatory pathways would produce identical activation from identical stimuli in different cell types. One could also conceive that the binding and the phosphorylation are completely independent events, in which case the kinase could phosphorylate NKCC1 in the absence of binding. If true, one has to conclude that the binding of the kinase to the cotransporter serves a function that is completely independent of phosphorylation. It is noteworthy that in PASK overexpression studies, Dowd and Forbush (18) detected a significant, small difference only at an intermediate activation level (preincubation in 30 mM extracellular Cl^-) but not at lower or maximal levels of activation. Thus, at maximal activation levels, the study of Dowd and Forbush (18) is in line with our finding of no significant change of transport activity. Finally, the overexpression of the dominant negative SPAK mutant in HEK293 cells in the study by Dowd and Forbush (18) might have produced indirect effects on NKCC1 activation. Their data using immunoprecipitated HA-SPAK on cotransporters are more difficult to reconcile with our experiments. It is possible that the coimmunoprecipitations (NKCC1 or HA-SPAK) could have pulled down another kinase that directly phosphorylates NKCC1. We have evidence in this study of additional kinases that interact with SPAK (see below). However, if these kinases

TABLE I

Summary of yeast two-hybrid screening with the binding domain (C terminus) of SPAK

The 1st column lists the mouse clones identified as positive interactors of SPAK. The 2nd column indicates the length of the mouse protein (in number of residues). The 3rd column reports the number of times each clone was isolated. The 4th column includes the range of the LacZ values (out of 139 clones measured, the average LacZ was 5 ± 6). The 5th column lists the independent clones isolated for each interacting protein: the beginning of the library clone amino acid sequence, its position within the protein, and in parentheses the number of times the clone was isolated. In the last column, we list the SPAK motifs identified within the interacting protein. The number in brackets indicates the position of the first residue within the protein. Asterisk, the motif was tested for interaction with SPAK using yeast two-hybrid assay, and the interaction was positive.

INTERACTING PROTEINS	LENGTH	#	LAC Z	CLONE STARTS	SPAK MOTIFS
Apoptosis-associated TK (AATYK)	1317	7	3.6 – 36.1	EDSEEE… 1127 (4)	RFTVs [1279]* RFSIt [1289]*
				SEPTFG… 961 (1)	
				PLRAGH… 1223 (1)	
				SEVLSP… 1003 (1)	
Gelsolin	731	6	5.0 – 16.8	LFQVR… 514 (1)	RFVIe [627]
				LFGGKP… 487 (1)	
				EESGSE… 582 (2)	
				AVEVMP… 527 (1)	
				ASSSG… 519 (1)	
Otoferlin	1997	2	8.4 – 41.3	NQSPGL… 1386 (2)	
WNK4	954	2	6.1 – 19.9	PSSLLP… 579 (2)	RFQVt [728]
heat shock protein 105	859	1	4.1	PYPEA… 473 (1)	RFVVq [461]
Novel tyrosine kinase *Similar to AATYK*	1307	7	3.6-16.8	REAPVP… 1108 (1)	RFSVs [1234]
				ETPTN… 1166 (2)	
				EPSTPP… 1183 (1)	
				ANGVLM… 904 (1)	
				GTPEGD… 1176 (1)	
				GSRGPG… 1100 (1)	
Colon cancer antigen 43		4	10.9-12.5		

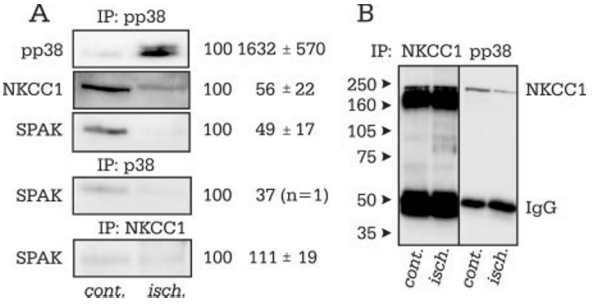

FIG. 9. *A*, coimmunoprecipitation experiments with control (*cont.*) and ischemic (*isch.*) brain samples showing decreased interaction between NKCC1 and p38 upon ischemic stress. Phosphorylated p38 (*pp38*), p38, or NKCC1 were immunoprecipitated (*IP*) from brain samples, and immunoprecipitates were tested by Western blot analysis for pp38 (positive control), NKCC1, and SPAK. Values shown on the *right* represent quantitation of the bands obtained by scanning densitometry. Values for ischemic brain sample are relative to control brain samples. They represent the mean ± S.E. ($n = 4$), except when indicated. *B*, immunoprecipitation experiment showing that only larger molecular weight NKCC1 (phosphorylated NKCC1) is immunoprecipitated by pp38.

are brought into contact with the cotransporter via SPAK binding, disrupting the interaction of the scaffolding protein should disrupt the availability of the associated kinase and thus affect the activity of the flux. Further work is needed to address this issue and reconcile these data.

Immunofluorescence studies revealed that SPAK expression in the nervous system is far more abundant than OSR1 expression. OSR1 is generally found in structures similar to those expressing SPAK, but at much lower levels (data not shown). As shown in our previous study, SPAK expression is highest in choroid plexus, solely localized on the apical membrane (Fig. 8*A*). Apical expression coincides with NKCC1 (13, 27, 28). In spinal cord, the kinase is found in both white and gray matter, a pattern that correlates well with KCC3 staining (20). In the nerve fiber, abundant SPAK expression is found in the node of Ranvier, where NKCC1 is abundantly expressed (26). Thus, SPAK expression seems to correlate tightly with cation-chloride cotransporter expression. Outside the choroid plexus, SPAK is found in the brain and mostly in brain stem structures, with the most prominent labeling seen in the spinal tract of the 5th nerve and in the auditory nuclei of the medial nucleus of the trapezoid and the cochlear nucleus. Our immunofluorescence data therefore agree with the conclusions of Ushiro *et al*. (15) that SPAK is rich in epithelia and neurons and add more detailed information about SPAK-positive nuclei. The question of why SPAK expression is high specifically in the aforementioned nuclei remains to be solved.

By using the extreme carboxyl terminus of SPAK as a bait in a yeast two-hybrid screen, we identified several interesting proteins as interacting candidates of SPAK/OSR1 as follows: HSP105, a heat shock protein that was originally cloned based on its marked up-regulation by dehydration in the renal medulla (29, 30); gelsolin, an actin-binding protein that protects against stress when overexpressed (31) and that is depleted in cells after oxidative injury (32); otoferlin, a protein originally cloned from inner ear (33) with alternatively spliced isoforms in brain, believed to be involved in membrane trafficking in a Ca^{2+}-dependent manner (such as synaptotagmin) (34); a tyrosine kinase (AATYK) that is related to the apoptotic pathway (35); a novel tyrosine kinase with unidentified function but related to AATYK; and WNK4 a kinase that has been implicated in hypertension (36) and that is involved in regulating trafficking of the Na-Cl cotransporter (37). Together with the study by Johnston *et al.* (38) and our demonstration by coimmunoprecipitation that SPAK interacts with p38, these

newly identified interactor candidates of SPAK strongly suggest a role for this Ste20 kinase in cellular stress.

Consistent with our hypothesis that SPAK and OSR1 function as scaffolding proteins is the observation that the two stress-related proteins exist in two forms in cells: a large molecular weight form that conserves the catalytic domain of the kinase, and a lower molecular weight form with a truncated catalytic domain. For SPAK, it is only in brain tissue that the large molecular weight form is far more abundant than the lower molecular form. For OSR1, which is phylogenetically older than SPAK, the truncated form is more abundant than the full-length form. This suggests either an important regulatory role as a native "dominant negative" kinase or a function of the protein that is completely independent of kinase activity. It is of interest to note that the second methionine is conserved in amphibians and in *Drosophila* but is substituted by leucine, isoleucine, or valine residues in *C. elegans* and plants. The prevalence of the shorter version is therefore likely to represent an adaptation process of OSR1 in higher organisms such as amphibians, insects, and mammals.

Strong support for the notion that SPAK and OSR1 might function as scaffolding proteins stems from our demonstration that SPAK interaction with NKCC1 (amount of SPAK coimmunoprecipitated with NKCC1) is not affected by cellular stress, such as ischemic stress, whereas the interaction of p38 with SPAK (p38 coimmunoprecipitated with SPAK) and with NKCC1 (p38 coimmunoprecipitated with NKCC1) is significantly reduced upon stress.

Together with the fact that SPAK expression was shown to highly correlate with NKCC1 (on the apical membrane of choroid plexus, on the basolateral membrane of salivary epithelial cells, at the node of Ranvier) and NKCC2 (apical membrane of thick ascending limb of Henle, data not shown) under normal non-stress conditions, our data suggest that SPAK might play a scaffolding role. We suggest that SPAK/OSR1 gather stress-related proteins in the proximity of cation-chloride cotransporters and, as we have shown here for phosphorylated p38 and SPAK, release proteins upon stress stimuli. It is therefore tempting to speculate that the cotransporters might play a sensing and/or transducing role in the response of cells to environmental stress.

Acknowledgment—We thank N. Byun for providing the teased sciatic nerve preparations.

REFERENCES

1. Delpire, E., and Mount, D. B. (2002) *Annu. Rev. Physiol.* **64,** 803–843
2. Hebert, S. C., Mount, D. B., and Gamba, G. *Pfluegers Arch.*, in press
3. Kaplan, M. R., Mount, D. B., Delpire, E., Gamba, G., and Hebert, S. C. (1996) *Annu. Rev. Physiol.* **58,** 649–668
4. Topper, J. N., Wasserman, S. M., Anderson, K. R., Cai, J., Falb, D., and Gimbrone, M. A., Jr. (1997) *J. Clin. Investig.* **15,** 2941–2949
5. Sun, D., Lytle, C., and O'Donnell, M. E. (1997) *Am. J. Physiol.* **272,** C1829–C1835
6. Russell, J. M. (2000) *Physiol. Rev.* **80,** 211–276
7. Lauf, P. K., Bauer, J., Adragna, N. C., Fujise, H., Zade-Oppen, A. A. M., Ryu, K., and Delpire, E. (1992) *Am. J. Physiol.* **263,** C917–C932
8. Flatman, P. W., and Creanor, J. (1999) *J. Physiol. (Lond.)* **519,** 143–152
9. Panet, R., Marcus, M., and Atlan, H. (2000) *J. Cell Physiol.* **182,** 109–118
10. Shen, M.-R., Chou, C.-Y., Hsu, K.-F., Liu, H.-S., Dunham, P. B., Holtzman, E. J., and Ellory, J. C. (2001) *Proc. Natl. Acad. Sci. U. S. A.* **98,** 14714–14719
11. Loffing, J., Loffing-Cueni, D., Hegyi, I., Kaplan, M. R., Hebert, S. C., Le Hir, M., and Kaissling, B. (1996) *Kidney Int.* **50,** 1180–1190
12. Kim, J. A., Kang, Y. S., Park, S. H., Kim, H. W., Cho, S. Y., and Lee, Y. S. (2001) *Eur. J. Pharmacol.* **433,** 1–6
13. Piechotta, K., Lu, J., and Delpire, E. (2002) *J. Biol. Chem.* **277,** 50812–50819
14. Dan, I., Watanabe, N. M., and Kusumi, A. (2001) *Trends Cell Biol.* **11,** 220–230
15. Ushiro, H., Tsutsumi, T., Suzuki, K., Kayahara, T., and Nakano, K. (1998) *Arch. Biochem. Biophys.* **355,** 233–240
16. Tamari, M., Daigo, Y., and Nakamura, Y. (1999) *J. Hum. Genet.* **44,** 116–120
17. Leiserson, W. M., Harkins, E. W., and Keshishian, H. (2000) *Neuron* **28,** 793–806
18. Dowd, B. F., and Forbush, B. (2003) *J. Biol. Chem.* **278,** 27347–27353
19. Strange, K., Singer, T. D., Morrison, R., and Delpire, E. (2000) *Am. J. Physiol.* **279,** C860–C867
20. Pearson, M., Lu, J., Mount, D. B., and Delpire, E. (2001) *Neuroscience* **103,** 483–493
21. James, P., Halladay, J., and Craig, E. A. (1996) *Genetics* **144,** 1425–1436
22. Lu, J., Karadsheh, M., and Delpire, E. (1999) *J. Neurobiol.* **39,** 558–568
23. Kaplan, M. R., Plotkin, M. D., Brown, D., Hebert, S. C., and Delpire, E. (1996) *J. Clin. Investig.* **98,** 723–730
24. Darman, R. B., Flemmer, A., and Forbush, B. I. (2001) *J. Biol. Chem.* **276,** 34359–34362
25. Darman, R. B., and Forbush, B. (2002) *J. Biol. Chem.* **277,** 37542–37550
26. Alvarez-Leefmans, F. J., Leon-Olea, M., Mendoza-Sotelo, J., Alvarez, F. J., Anton, B., and Garduno, R. (2002) *Neuroscience* **104,** 569–582
27. Plotkin, M. D., Kaplan, M. R., Peterson, L. N., Gullans, S. R., Hebert, S. C., and Delpire, E. (1997) *Am. J. Physiol.* **272,** C173–C183
28. Wu, Q., Delpire, E., Hebert, S. C., and Strange, K. (1998) *Am. J. Physiol.* **275,** C1565–C1572
29. Kojima, R., Randall, J., Brenner, B. M., and Gullans, S. R. (1996) *J. Biol. Chem.* **271,** 12327–12332
30. Santos, B. C., Chevaile, A., Kojima, R., and Gullans, S. R. (1998) *Am. J. Physiol.* **274,** F1054–F1061
31. Koya, R. C., Fujita, H., Shimizu, S., Ohtsu, M., Takimoto, M., Tsujimoto, Y., and Kuzumaki, N. (2000) *J. Biol. Chem.* **275,** 15343–15349
32. Christofidou-Solomidou, M., Scherpereel, A., Solomides, C. C., Muzykantov, V. R., Machtay, M., Albelda, S. M., and DiNubile, M. J. (2002) *Lung* **180,** 91–104
33. Yasunaga, S., Grati, M., Cohen-Salmon, M., El-Amraoui, A., Mustapha, M., Salem, N., El-Zir, E., Loiselet, J., and Petit, C. (1999) *Nat. Genet.* **21,** 363–369
34. Varga, R., Kelley, P. M., Keats, B. J., Starr, A., Leal, S. M., Cohn, E., and Kimberling, W. J. (2003) *J. Med. Genet.* **40,** 45–50
35. Tomomura, M., Hasegawa, Y., Hashikawa, T., Tomomura, A., Yuzaki, M., Furuichi, T., and Yano, R. (2003) *Brain Res. Mol. Brain Res.* **112,** 103–112
36. Monti, J., Zimdahl, H., Schulz, H., Plehm, R., Ganten, D., and Hubner, N. (2003) *Hypertension* **41,** 938–942
37. Wilson, F. H., Kahle, K. T., Sabath, E., Lalioti, M. D., Rapson, A. K., Hoover, R. S., Hebert, S. C., Gamba, G., and Lifton, R. P. (2003) *Proc. Natl. Acad. Sci. U. S. A.* **100,** 680–684
38. Johnston, A. M., Naselli, G., Gonez, L. J., Martin, R. M., Harrison, L. C., and Deaizpurua, H. J. (2000) *Oncogene* **19,** 4290–4297